where

$$f_3 = t^{-1} J_1\left(\frac{\gamma v}{2} t\right) u_{-1}(t), \tag{30}$$

$$f_4 = \frac{4}{\gamma^2 v^2}(t-2)(t+2)^{-1} J_2\left(\frac{\gamma v}{2}[t^2-4]^{1/2}\right) u_{-1}(t-2). \tag{31}$$

When $t < 2$, f_3 represents the reflected wave at the input end before the first reflection returns. Fig. 3 shows the time domain scattering reflection parameter $S_{11}(t)$ for two impedance ratios $Z_L/Z_S = 4, 9$. Note that $S_{11}(t)$ is normalized with respect to a factor $\ln(Z_L/Z_S)$. The drop of $S_{11}(t)$ at $t = 2$ is 0.25 for both impedance ratios. Equations (24) and (29) reveal that $S_{21}(t)$ is an even function of γ while $S_{11}(t)$ is an odd function of γ.

IV. Conclusion

Exact solutions are found for both the frequency domain and time domain scattering parameters of an exponential transmission line. The time domain scattering parameters of an exponential line lay the foundation for the studies of interaction between nonuniform lines and linear/nonlinear loads, and pulse waveform alteration in the time domain.

References

[1] C. T. Tai, "Transients on lossless terminated transmission lines," *IEEE Trans. Antennas Propagat.*, vol. AP-26, pp. 556–561, July 1978.

[2] J. E. Schutt-Aine and R. Mittra, "Scattering parameter transient analysis of transmission lines loaded with nonlinear terminations," *IEEE Trans. Microwave Theory Tech.*, vol. 36, pp. 529–536, Mar. 1988.

[3] A. R. Djordjevic, T. K. Sarkar, and R. F. Harrington, "Analysis of transmission lines with arbitrary nonlinear terminal networks," *IEEE Trans. Microwave Theory Tech.*, vol. MTT-21, pp. 660–666, June 1986.

[4] H. Mohammadian and C. T. Tai, "A general method of transient analysis for a lossless transmission line and its analytical solution to time-varying resistive terminations," *IEEE Trans. Antennas Propagat.*, vol. AP-32, pp. 309–312, Mar. 1984.

[5] Q. Gu and J. A. Kong, "Transient analysis of single and coupled lines with capacitively-loaded junctions," *IEEE Trans. Microwave Theory Tech.*, vol. MTT-34, pp. 952–964, Sept. 1986.

[6] C.-W. Hsue, "Elimination of ring signals for a lossless, multiple-section transmission line," *IEEE Trans. Microwave Theory Tech.*, vol. 37, pp. 1178–1183, Aug. 1989.

[7] I. L. Hill and D. Mathews, "Transient analysis of systems with exponential lines," *IEEE Trans. Microwave Theory Tech.*, vol. MTT-25, pp. 777–783, Sept. 1977.

[8] E. R. Schatz and E. M. Williams, "Pulse transients in exponential transmission lines," *Proc. I.R.E.*, vol. 27, pp. 65–71, Oct. 1950.

[9] R. J. Veghte and C. A. Balanis, "Dispersion of transient signals in microstrip transmission lines," *IEEE Trans. Microwave Theory Tech.*, vol. MTT-34, pp. 1427–1436, Dec. 1986.

[10] C. D. Hechtman and C.-W. Hsue, "Transient analysis of a step wave propagating in a lossy dielectric," *J. Appl. Phys.*, vol. 65, pp. 3335–3339, May 1989.

[11] ____, "Time domain scattering parameters for a lossy dielectric," *J. Appl. Phys.*, vol. 67, pp. 2199–2209, Mar. 1990.

[12] G.-C. Liang, Y.-W. Liu, and K. K. Mei, "Full-wave analysis of coplanar waveguide and slotline using the time-domain finite-difference method," *IEEE Trans. Microwave Theory Tech.*, vol. 37, pp. 1949–1957, Dec. 1989.

[13] W. C. Johnson, *Transmission Lines and Networks*. New York: McGraw-Hill, 1950.

[14] A. Erdelyi *et al.*, *Table of Integral Transforms*. New York: McGraw-Hill, 1954.

Analysis of 3-D Microwave Resonators using Covariant-Projection Elements

J. P. Webb and Ruth Miniowitz

***Abstract*—Three-dimensional microwave resonators of arbitrary shape can be analyzed with the finite element method using covariant-projection elements, curvilinear bricks which impose only tangential field continuity. The method produces no spurious modes, and works well even when sharp metal edges are present. The matrices involved, though large, are sparse; an appropriate sparse eigenvalue algorithm allows the method to run in modest amounts of memory. Results are presented for a number of test cases, including a rectangular microstrip resonator.**

I. Introduction

ELECTROMAGNETIC resonance is important in the operation of many microwave devices, and its prediction has been the subject of a large number of papers. For structures of arbitrary shape, numerical methods are necessary. The finite element method has long been used for finding the modes of uniform waveguides [1], and has been proposed as a technique for 3-D cavity resonance [2], [3]. However, several obstacles have impeded the application of 3-D elements. The problem of spurious modes has, rightly, received the most attention, and the last few years have seen the publication of a variety of solutions, both in 2-D and in 3-D [2]–[7]. However, a second difficulty which arises commonly in microwave devices is that of sharp conducting edges and corners. To find resonances, it is usually necessary to solve for the electric or magnetic field directly, and these fields are, in general, infinite at sharp edges. The continuous, piecewise-polynomial variations provided by conventional finite elements do not adequately represent such singularities, and lead to poor results [8], [9].

One answer is to add to the polynomials special trial functions capable of modeling the singularity [8]. A different, and in many ways more elegant, solution is provided by the work of Crowley *et al.* [10], [11] on new finite elements capable of avoiding spurious modes. These are called covariant-projection elements. Covariant-projection elements only enforce the tangential continuity of the vector field, leaving the normal component at interfaces free to adopt its natural value. This reduced continuity appears to allow a better modeling of singularities. A version of the elements was tried in 2-D for the analysis of uniform waveguides with sharp edges, with excellent results [12]. Crowley *et al.* demonstrated the validity of the brick element for several 3-D cavity problems, but none had sharp metal edges. It is the purpose of this paper to show that covariant-projection elements, combined with a suitable sparse-matrix solution of the algebraic problem, is an effective method for 3-D cavity resonance, even when singularities are present.

Manuscript received November 5, 1990; revised June 27, 1991. This work was supported by the Natural Sciences and Engineering Research Council of Canada.

J. P. Webb is with the Computational Analysis and Design Laboratory, Department of Electrical Engineering, McGill University, 3480 University Street, Montreal, PQ H3A 2A7, Canada.

R. Miniowitz was with the Computational Analysis and Design Laboratory, Department of Electrical Engineering, McGill University, Montreal, PQ, Canada. She is currently with the Electromagnetics Department, RAFAEL, P.O. Box 2250, Haifa 31021, Israel.

IEEE Log Number 9102822.

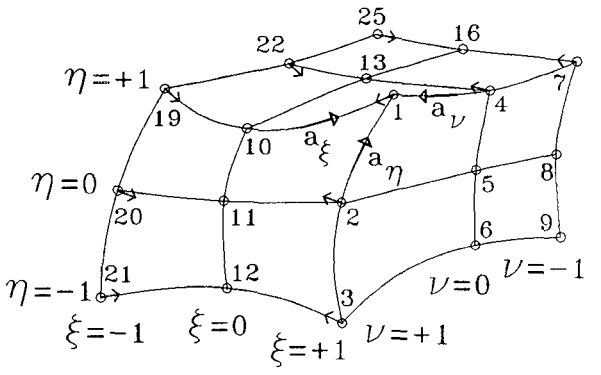

Fig. 1. A 3-D Covariant-Projection Element. There are 27 nodes; 19 of them appear as numbered circles on the three faces visible in the above view. There are 18 degrees of freedom (three planes of six) for the ξ-component; 10 of them are represented by small arrows.

II. Finite Element Analysis

The basic approach to the finite element analysis of electromagnetic resonance is well established. The resonant magnetic fields $\boldsymbol{H}$ are the stationary points of a functional $F(\boldsymbol{H})$ [13]. By first representing $\boldsymbol{H}$ as a linear combination of finite-element basis functions, the problem of finding the stationary points of F is reduced to an algebraic eigenvalue problem:

$$([S]-k_o^2[T])\{H\}=0 \tag{1}$$

where $\{H\}$ is a column vector of N unknown coefficients; $[S],[T]$ are $N\times N$ matrices; and k_o is the unknown resonant wavenumber.

This straightforward scheme, if used with conventional, Lagrangian finite elements, generates spurious modes. The reasons for this are discussed elsewhere [2], [14], [10], [12], as are various methods of eliminating the spurious modes. The method proposed by Crowley et al. is to use covariant-projection elements.

III. Covariant-Projection Elements

A 3-D covariant-projection element is shown in Fig. 1. Its geometry is the same as that of the curvilinear, isoparametric version of the rectangular, 27-node, Lagrange element ([15], Sections 7.20, 8.1 and 8.2). Each element has a local coordinate system ξ,η,ν that is not necessarily orthogonal, but nevertheless can be used to define unitary vectors [16] $\boldsymbol{a}_\xi,\boldsymbol{a}_\eta,\boldsymbol{a}_\nu$ at each point. The projections of a vector field $\boldsymbol{H}$ on the unitary vectors are called its *covariant* components. They are

$$H_\xi=\boldsymbol{H}\cdot\boldsymbol{a}_\xi;\qquad H_\eta=\boldsymbol{H}\cdot\boldsymbol{a}_\eta;\qquad H_\nu=\boldsymbol{H}\cdot\boldsymbol{a}_\nu. \tag{2}$$

At the edges of the element, these are proportional to the tangential components of $\boldsymbol{H}$. For example, if H_ξ is zero on the edge $\eta=\nu=1$, $\boldsymbol{H}$ is perpendicular to the edge. By using H_ξ, H_η and H_ν as the unknowns instead of H_x, H_y and H_z, it is easy to impose vector boundary conditions, and tangential continuity from one element to the next, even at curved boundaries.

After calculating the covariant components one can get the full vector $\boldsymbol{H}$ easily by using the reciprocal vectors, $\boldsymbol{a}^\xi,\boldsymbol{a}^\eta,\boldsymbol{a}^\nu$ defined as follows [16]:

$$\boldsymbol{a}^\xi=\frac{1}{V}(\boldsymbol{a}_\eta\times\boldsymbol{a}_\nu);\quad \boldsymbol{a}^\eta=\frac{1}{V}(\boldsymbol{a}_\nu\times\boldsymbol{a}_\xi);\quad \boldsymbol{a}^\nu=\frac{1}{V}(\boldsymbol{a}_\xi\times\boldsymbol{a}_\eta) \tag{3}$$

where V is $\boldsymbol{a}_\xi\cdot(\boldsymbol{a}_\eta\times\boldsymbol{a}_\nu)$. In terms of these vectors, the three-component $\boldsymbol{H}$ is

$$\boldsymbol{H}=H_\xi\boldsymbol{a}^\xi+H_\eta\boldsymbol{a}^\eta+H_\nu\boldsymbol{a}^\nu \tag{4}$$

The trial functions for H_ξ, H_η and H_ν are mixed-order; that is, each trial function for H_ξ is a polynomial of order 2 in η and order 2 in ν, but order 1 in ξ, and similarly for the other components (see Appendix). The mixing of orders seems to be important in eliminating spurious modes [11].

One of the properties of this kind of element is that it gives rise to zero-frequency solutions, most of which are of no physical significance. These are not spurious modes in the usual sense, because, having zero frequency, they are readily identified and avoided. By an argument similar to that used in 2-D [12], it is possible to predict the number M of nonphysical, zero-frequency modes: it is the number of nodes in the finite-element mesh of 27-node bricks, minus the number of nodes that lie on magnetic walls. The exception to this rule is if there is no magnetic wall in the problem, in which case M is just the number of nodes minus one.

TABLE I
Comparison of the Cut-Off Wavenumbers (rads/mm) for Different Methods, for a Double-Ridged Waveguide

		N	Mode 1	Mode 2	Mode 3
12 bricks 3D	$\boldsymbol{H}$	232	0.1443	0.6268	0.6880
	$\boldsymbol{E}$	324	0.1433	0.6211	0.6731
48 quads. 2D [12]	$\boldsymbol{H}$	624	0.1440	0.6200	0.6723
	$\boldsymbol{E}$	528	0.1437	0.6197	0.6721
TE scalar C^1 [26]			0.1440	0.6192	0.6713
Montgomery [27]			0.1437	0.6190	0.6712
Utsumi [28]			0.1438	0.6215	0.6707

IV. Computer Program

A FORTRAN computer program has been written using the covariant-projection elements described above. The integration required to calculate matrices $[S]$ and $[T]$ in (1) was carried out numerically, using a 27-point ($3\times3\times3$) Gauss method ([15], Section 8.9). The formulation for the electric field is very similar to that given above for the magnetic field, and the program can solve for either. Since only tangential continuity is enforced, there is no difficulty caused by the discontinuity of the normal component of the electric field at dielectric interfaces.

3-D problems involve large matrices. For example, in one of the problems below, the order of the matrices is $N=1828$. The memory required for $[S]$ and $[T]$ of this size is about 25 MB (8 bytes per entry, and taking into account that both matrices are symmetric). A dense-matrix eigenvalue solver therefore needs at least this much primary memory. Storing $[S]$ and $[T]$ on secondary memory (e.g., disk) is usually not a practical option because of the relatively long time taken to access data.

However, $[S]$ and $[T]$ are quite sparse: to store just the nonzero entries of both matrices, when $N=1828$, takes about 1 MB. An eigenvalue solver that can work with matrices stored in this form can reduce considerably the memory requirements. For the most part, sparse eigenvalue solvers in finite-element analysis have used some variant of subspace iteration [17], which efficiently finds the few lowest or highest eigenvalues. In the present case, such an approach is not possible, because the

TABLE II
WAVENUMBERS (rads/m) OF THE FIRST SIX MODES OF THE DIELECTRIC-LOADED BOX IN [7]

		N	1	2	3	4	5	6
8 Bricks	H	224	5.483	7.836	10.701	10.896	12.083	12.773
	E	160	5.326	8.376	10.818	11.210	12.225	13.142
64 Bricks	H	1664	5.435	7.829	9.969	10.644	11.630	12.444
	E	1408	5.378	7.834	9.970	10.669	11.639	12.457
64 Bricks [22], [23]	H	1120	5.460	7.860	9.986	10.664	11.623	12.442
	E	928	5.388	7.815	9.917	10.636	11.602	12.410
C^0 [7]	H	603	5.60	9.96	12.38	12.55	13.43	14.31

lowest M eigenvalues are all zero, and the eigenvalues of interest lie somewhere in the middle of the spectrum. We used another technique [18], which consists of repeated factorization of $[S]-\lambda[T]$ by a profile method, iterating on λ until the required eigenvalues have been found. Inverse iteration then computes the eigenvectors. The algorithm is able to find p consecutive eigenvalues, starting with the kth; in our case, we set $k=M+1$ to avoid the zero-frequency modes. Notice that it is important to have a reliable estimate for M.

The examples below were run on MicroVax II and HP9000 Series 500 computers. The largest problem needed less than 8 MB of primary memory.

V. RESULTS

The first results are for uniform waveguides, which can be solved in 2-D, but were solved here in 3-D. Details of the waveguides and their analysis with 2-D finite elements may be found in [12]. To find the cut-off frequencies, we modeled the cross-section of the waveguide in the xy plane and extruded it a small distance in the z-direction. The two end planes (perpendicular to the z-axis) were taken as magnetic walls when modeling modes which are TE at cut-off, and as electric walls when modeling modes which are TM at cut-off. To find the resonant frequencies when the propagation constant, β, is not zero, we set the length of the waveguide equal to $\pi/(2\beta)$, and made one end plane an electric wall and the other a magnetic wall. In this way, each resonance corresponded to a mode whose quarter-wavelength was $\pi/(2\beta)$, i.e., whose propagation constant was β. (Occasionally a resonance corresponded to a mode for which *three*-quarters of a wavelength is equal to $\pi/(2\beta)$, but these were readily detected).

The first example is a double-ridged waveguide with two planes of symmetry and four sharp edges [12]. We modeled one quarter of the cross-section, with boundary conditions for the odd modes. Both $\boldsymbol{E}$ and $\boldsymbol{H}$ formulations were tried. Table I shows the cut-off frequencies obtained in 3-D with 12 brick elements, compared with results from other sources. N is the number of degrees of freedom.

In addition, the double-ridged waveguide was analyzed at nonzero values of β with 24 bricks (12 per layer). The frequencies agreed to two or three digits with the values predicted by the dispersion relation

$$k_o^2=\beta^2+k_c^2$$

when k_c was taken as the value given by the program for $\beta=0$.

The second waveguide problem is a shielded microstrip line, shown inset in Fig. 2. We analyzed one half of the line, with a magnetic wall on the plane of symmetry. Again, both $\boldsymbol{E}$ and $\boldsymbol{H}$ formulations were tried. Fig. 2 gives dispersion curves for the first 3 modes, using the $\boldsymbol{H}$ formulation and 16 elements in two layers (428 degrees of freedom). The solid lines are the results of a 2-D analysis [12]. The broken lines are non-finite-element results: the first mode is from [19]; and the other two are from [20]. The squares, triangles and diamonds are the 3-D finite-element results. There is good agreement between the different methods.

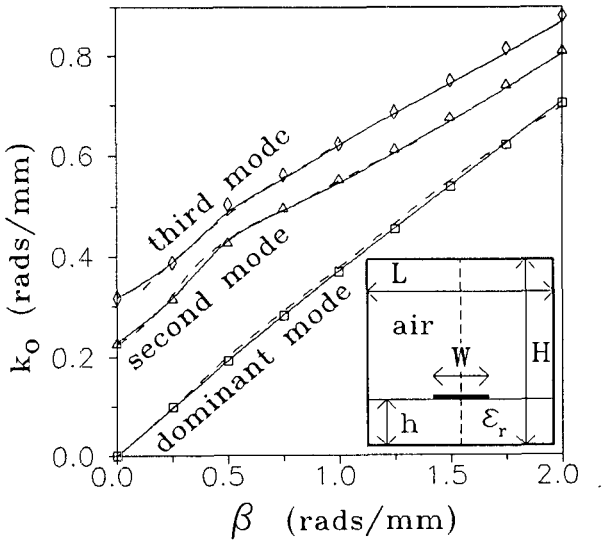

Fig. 2. Dispersion curves for the first three modes of a shielded microstrip transmission line. The broken line in the inset figure shows the plane of symmetry. $L=12.7$ mm, $W=1.27$ mm, $h=1.27$ mm, $H=12.7$ mm and $\epsilon_r=8.875$.

A truly three-dimensional example is the dielectric-loaded cavity described in [7]. Although there are no sharp metal edges, the dielectric corner and edges give rise to milder singularities [21]. Table II shows the resonant wave numbers for the first six modes. There is good agreement with results obtained with another finite-element method [22], [23], a 3-D version of the technique reported in [24]. This method uses a scalar potential in addition to a vector field modeled with conventional Lagrangian (C^0) elements. The frequencies predicted by the finite-element method of [7] are mostly quite different, partly because of the lower number of degrees of freedom, but probably also because of the use of Lagrangian elements, which do not model the singularities adequately.

The last example is a microstrip resonator, shown in Fig. 3. We analyzed one quarter of the problem, with boundary condi-

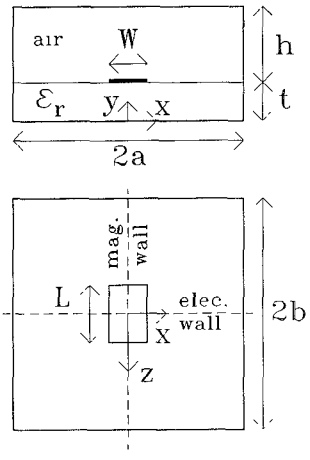

Fig. 3. A Microstrip Resonator: cross-section and plan views. $\epsilon_r = 9.47$, $W = 0.575$ mm, $h = 10$ mm, $t = 0.6$ mm, $a = b = 10$ mm, $L = 4.889$ mm. The strip was taken to be infinitely thin. The broken lines represent planes of symmetry.

TABLE III
WAVENUMBERS (rads/mm) OF THE FIRST TWO MODES OF THE MICROSTRIP STRUCTURE IN FIG. 3

		N	Mode 1	Mode 2
64 Bricks	H	1828	0.2319	0.3382
	E	1252	0.2336	0.3360
Uwano [25]			0.2304	—

tions for the dominant mode. Sixty-four bricks were used, in a $4\times4\times4$ arrangement, with smaller bricks near the sharp edges. Table III shows agreement between the finite-element results and those of a spectral domain method [25].

VI. Conclusion

Covariant-projection elements are capable of analyzing a wide variety of 3-D microwave resonators, including those with field singularities. Combined with sparse-matrix techniques, the method can be used on medium-range computers with modest amounts of memory.

Acknowledgment

The authors express their gratitude to C. Crowley, both for inspiring us to pursue further the application of covariant-projection elements, and for providing us with matrix-assembly subroutines for the 3-D element.

Appendix

In each element, the magnetic field is interpolated as follows:

$$\boldsymbol{H} = \sum_{t=1}^{18} H_{\xi t} X_t(\xi,\eta,\nu)\boldsymbol{a}^{\xi} + H_{\eta t} Y_t(\xi,\eta,\nu)\boldsymbol{a}^{\eta} + H_{\nu t} Z_t(\xi,\eta,\nu)\boldsymbol{a}^{\nu}$$

where X_t, Y_t, Z_t are polynomial trial functions, each of which is based at one of the 27 nodes of the brick, in the sense that it takes the value 1 at that node, and vanishes at many (but not all) of the other nodes. Table IV gives the polynomial for each X_t, together with the node at which it is based. In the table, l_1, l_2, q_1, q_2, and q_3 are Lagrange polynomials of degree one and two:

$$l_1(s) = \frac{1}{2}(1-s); \qquad l_2(s) = \frac{1}{2}(1+s)$$

$$q_1(s) = \frac{1}{2}s(s-1); \qquad q_2(s) = (1-s^2);$$

$$q_3(s) = \frac{1}{2}s(s+1).$$

TABLE IV
TRIAL FUNCTIONS X_t

i	X_t	Node	i	X_t	Node
1	$l_2(\xi)q_3(\eta)q_3(\nu)$	1	10	$l_1(\xi)q_3(\eta)q_3(\nu)$	19
2	$l_2(\xi)q_2(\eta)q_3(\nu)$	2	11	$l_1(\xi)q_2(\eta)q_3(\nu)$	20
3	$l_2(\xi)q_1(\eta)q_3(\nu)$	3	12	$l_1(\xi)q_1(\eta)q_3(\nu)$	21
4	$l_2(\xi)q_3(\eta)q_2(\nu)$	4	13	$l_1(\xi)q_3(\eta)q_2(\nu)$	22
5	$l_2(\xi)q_2(\eta)q_2(\nu)$	5	14	$l_1(\xi)q_2(\eta)q_2(\nu)$	23
6	$l_2(\xi)q_1(\eta)q_2(\nu)$	6	15	$l_1(\xi)q_1(\eta)q_2(\nu)$	24
7	$l_2(\xi)q_3(\eta)q_1(\nu)$	7	16	$l_1(\xi)q_3(\eta)q_1(\nu)$	25
8	$l_2(\xi)q_2(\eta)q_1(\nu)$	8	17	$l_1(\xi)q_2(\eta)q_1(\nu)$	26
9	$l_2(\xi)q_1(\eta)q_1(\nu)$	9	18	$l_1(\xi)q_1(\eta)q_1(\nu)$	27

References

[1] P. Daly, "Hybrid-mode analysis of microstrip by finite-element methods," *IEEE Trans. Microwave Theory Tech.*, MTT-19, pp. 19–25, Jan. 1971.

[2] J. P. Webb, "The finite element method for finding the modes of dielectric-loaded cavities," *IEEE Trans. Microwave Theory Tech.*, MTT-33, no. 7, pp. 635–639, July 1985.

[3] A. Konrad, "A direct three-dimensional finite element method for the solution of electromagnetic fields in cavities," *IEEE Trans. Magn.*, MAG-21, no. 6, pp. 2276–2279, Nov. 1985.

[4] B. M. A. Rahman, and J. B. Davies, "Penalty function improvement of waveguide solution by finite elements," *IEEE Trans. Microwave Theory Tech.*, MTT-32, no. 8, pp. 922–928, Aug. 1984.

[5] K. Hayata, M. Koshiba, M. Eguchi, and M. Suzuki, "Vectorial finite-element method without any spurious solutions for dielectric waveguiding problems using transverse magnetic-field component," *IEEE Trans. Microwave Theory Tech.*, MTT-34, no. 11, pp. 1120–1124, Nov. 1986.

[6] A. J. Kobelansky and J. P. Webb, "Eliminating spurious modes in finite-element waveguide problems by using divergence-free fields," *Electron Lett.*, vol. 22, no. 11, pp. 569–570, May 22, 1986.

[7] J. P. Webb, "Efficient generation of divergence-free fields for the finite element analysis of 3D cavity resonances," *IEEE Trans. Magn.*, MAG-24, no. 1, pp. 162–165, Jan. 1988.

[8] ____, "Finite element analysis of dispersion in waveguides with sharp metal edges," *IEEE Trans. Microwave Theory Tech.*, MTT-36, pp. 1819–1824, Dec. 1988.

[9] M. Israel, R. Miniowitz, "Hermitian finite-element method for inhomogeneous waveguides," *IEEE Trans. Microwave Theory Tech.*, MTT-38, no. 9, pp. 1319–1327, Sept. 1990.

[10] C. W. Crowley, P. P. Silvester, and H. Hurwitz, "Covariant projection elements for 3D vector field problems," *IEEE Trans. Magn.*, MAG-24, no. 1, pp. 397–400, Jan. 1988.

[11] C. W. Crowley, "Mixed order covariant projection finite elements for vector fields," Ph.D. dissertation, McGill University, Montreal, PQ, Canada, 1988.

[12] R. Miniowitz and J. P. Webb, "Covariant-projection quadrilateral elements for the analysis of waveguides with sharp edges," *IEEE Trans. Microwave Theory Tech.*, MTT-39, no. 3, pp. 501–505, Mar. 1991.

[13] A. D. Berk, "Variational principles for electromagnetic resonators and waveguides," *IRE Trans.*, AP-4, pp. 104–110, April, 1956.

[14] S. H. Wong and Z. J. Cendes, "Numerically stable finite element methods for the Galerkin solution of eddy current problems," *IEEE Trans. Magn. MAG-25*, no. 4, pp. 3019–3021, July 1989.

[15] O. C. Zienkiewicz, *The Finite-Element Method*, 3rd ed., London: McGraw-Hill, 1977.

[16] J. A. Stratton, *Electromagnetic Theory*. New York: McGraw-Hill, 1941.

[17] B. N. Parlett, *The Symmetric Eigenvalue Problem*. Englewood Cliffs, NJ: Prentice-Hall, 1980.
[18] H. R. Schwartz, *Fortran-Programme zur Methode der finiten elemente*. Stuttgart, Germany, B. G. Teubner, 1981.
[19] R. Mittra and T. Itoh, "A new technique for the analysis of the dispersion characteristics of microstrip lines," *IEEE Trans. Microwave Theory Tech.*, MTT-19, no. 1, pp. 47–56, Jan. 1971.
[20] D. Mirshekar-Syahkal and J. Brian Davies, "Accurate solution of microstrip and coplanar structures for dispersion and for dielectric and conductor losses," *IEEE Trans. Microwave Theory Tech.*, MTT-27, no. 7, pp. 694–699, July 1979.
[21] R. De Smedt, "Singular field behaviour near the tip of a dielectric or dielectric-metallic corner," *Radio Science*, vol. 22, no. 7, pp. 1190–1196, Dec. 1987.
[22] I. Bardi, private communication, 1990.
[23] I. Bardi, O. Biro, and K. Preis, "Finite element scheme for 3D cavities without spurious modes," in Proc. European *TEAM Workshop and International Seminar on Electromagnetic Field Analysis*, Oxford, England, April 23–25, 1990, pp. 255–265.
[24] I. Bardi and O. Biro, "Improved finite element formulation for dielectric loaded waveguides," *IEEE Trans. Magn.*, MAG-26, no. 2, pp. 450–453, Mar. 1990.
[25] T. Uwano, "Accurate characterization of microstrip resonator open end with new current expression in spectral-domain approach," *IEEE Trans. Microwave Theory Tech.*, MTT-37, no. 3, pp. 630–633, Mar. 1989.
[26] M. Israel and R. Miniowitz, "An efficient finite element method for nonconvex waveguide based on Hermitian polynomials," *IEEE Trans. Microwave Theory Tech.*, MTT-35, no. 11, pp. 1019–1026, Nov. 1987.
[27] J. P. Montgomery, "On the complete eigenvalue solution of ridged waveguide," *IEEE Trans. Microwave Theory Tech.*, MTT-19, pp. 547–555, June 1971.
[28] Y. Utsumi, "Variational analysis of ridged waveguide modes," *IEEE Trans. Microwave Theory Tech.*, MTT-33, pp. 111–120, Feb. 1985.

Microwave Hall Effect in a TE_{11p} Cylindrical Cavity

A. Y. Al Zoubi

Abstract—**A microwave Hall effect signal produced by a TE_{11p} degenerate cylindrical cavity is considered. The analysis presented identifies the cavity end walls as the source of the Hall signal, and a formula is derived relating the Hall output power to the dimensions of the cavity. Experimental results from the measurement of the empty cavity signal at 9.5 GHz are reported.**

I. Introduction

The microwave Hall effect method has recently been introduced in measurements of the mobility values of metals [1]. The method utilizes a resonant cavity with doubly degenerate modes. When a static magnetic field is applied in the direction of the symmetry axis, the electrical conductivity of the metal ceases to be scalar and becomes tensorial. The tensorial conductivity connects the otherwise mutually independent modes of the cavity and results in power transfer from the input port to the output port. This power transfer is usually referred to as the empty-cavity signal. Theoretical analysis has shown that an empty-cavity signal produced by a rectangular degenerate cavity operating at its fundamental modes is given as a function of cavity dimensions [1].

The microwave Hall effect method has been used extensively in the measurement of low Hall mobility values in a variety of materials [2]–[4]. The test sample is usually held at the cavity E-field antinode, and the Hall effect manifests itself as a rotation in the plane of polarization of the microwaves as they pass through the sample. However, the empty-cavity signal may obscure measurement of the Hall effect in low-mobility materials. This background signal is superimposed on the signal from the sample and may become dominant for materials of low mobility. The empty cavity signal must therefore be minimized in order to accurately measure the Hall effect in such materials.

In this paper, the Hall effect in the cavity end walls is described and a quantitative description of the empty cavity signal is given. The calculation is based on Slater's treatment [5] of the expanded electromagnetic fields in terms of the two orthogonal TE_{11p} modes in a cylindrical cavity. An expression for the empty-cavity signal is then formulated in terms of cavity dimensions. Experimental results from measurements at 9.5 GHz have been obtained.

II. Theory

The cavity treated in this paper is a cylindrical one in which only doubly degenerate TE_{11p} modes are excited. The cavity, of length d and radius a, is iris-coupled to matched waveguide transmission lines such that in principle there is complete isolation between input and output waveguides. The coupling slots S_1 and S_2 connect the cavity with the mutually orthogonal waveguides as shown in Fig. 1. In the absence of the magnetic field, the power fed from the oscillator to the cavity via waveguide 1 does not arrive at the receiver coupled to waveguide 2. If an external magnetic field, B, is applied along the z axis, then in addition to the dominant mode (I) excited in the cavity an additional mode (II) will be excited as a consequence of the Hall effect in the cavity end walls. A portion of the incident power, P_1, begins to arrive at the receiver; this is referred to as the empty-cavity Hall output power, P_2. The electromagnetic field in a cylindrical cavity operating in the TE_{11p} mode may be written as

$$E_r = (-E_0/k_c r) J_1(k_c r) \sin(p\pi z/d) \begin{cases} \sin\phi \\ \cos\phi \end{cases} \tag{1a}$$

$$E_\phi = E_0 J_1'(k_c r) \sin(p\pi z/d) \begin{cases} \cos\phi \\ \sin\phi \end{cases} \tag{1b}$$

$$H_r = (jp\pi E_0/\omega\mu_0 d) J_1'(k_c r) \cos(p\pi z/d) \begin{cases} \cos\phi \\ \sin\phi \end{cases} \tag{1c}$$

$$H_\phi = (jp\pi E_0/\omega\mu_0 k_c r) J_1(k_c r) \cos(p\pi z/d) \begin{cases} -\sin\phi \\ \cos\phi \end{cases} \tag{1d}$$

$$H_z = (jk_c E_0/\omega\mu_0) J_1(k_c r) \sin(p\pi z/d) \begin{cases} \cos\phi \\ \sin\phi \end{cases} \tag{1e}$$

where E_0 is the maximum electric field in the cavity, k_c the cutoff wavenumber, μ_0 the permeability of free space, and ω the angular frequency. $J_1(k_c r)$ is a cylindrical Bessel function of the first order and $J_1'(k_c r)$ is its first derivative. The total electric field, E, in the cavity may be expressed in the form of

Manuscript received June 18, 1990; revised April 4, 1991.
The author was with the Electrical Engineering Department, Nottingham University, U.K. He is now with the Electrical Engineering Department, Mutah University, P.O. Box 7, Karak, Jordan.
IEEE Log Number 9102320.